Biochemical and Biophysical Research Communications 418 (2012) 122–127

Contents lists available at SciVerse ScienceDirect

Biochemical and Biophysical Research Communications

journal homepage: www.elsevier.com/locate/ybbrc

Crystal structures of the *Arabidopsis thaliana* abscisic acid receptor PYL10 and its complex with abscisic acid

Demeng Sun [a,1], Haipeng Wang [a,1], Minhao Wu [a], Jianye Zang [a], Fangming Wu [b,*], Changlin Tian [a,b,*]

[a] Hefei National Laboratory for Physical Sciences at Microscale, School of Life Sciences, University of Science and Technology of China, Hefei, Anhui 230026, China
[b] High Magnetic Field Laboratory, Chinese Academy of Sciences, Hefei, Anhui 230031, China

ARTICLE INFO

Article history:
Received 8 December 2011
Available online 8 January 2012

Keywords:
ABA receptor
PYR/PYL/RCAR family
Phytohormone
Helix-grip fold
START domain

ABSTRACT

Abscisic acid (ABA) is one of the most essential phytohormones, and plays an important role in growth and development regulation, as well as in stress responses. The PYR/PYL/RCAR family (PYL for short)—comprised of 14 proteins in *Arabidopsis*—was recently identified as soluble ABA receptors that function in the perception and transduction of ABA signaling. In this work, the crystal structures of PYL10 were determined in the apo- and ABA-bound states, with respective resolutions of 3.0 and 2.7 Å. Surprisingly, a closed CL2 conformation was observed in the apo–PYL10 structure, which was different from a previously reported open CL2 conformation. A putative two-conformation dynamical equilibrium model was proposed to explain PYL10's constitutive binding to PP2Cs in the apo-state and its increased PP2C binding ability in the ABA-bound state.

1. Introduction

Abscisic acid is an important phytohormone that regulates numerous developmental processes and adaptive stress responses in plants [1,2]. The soluble ABA receptor family (PYR/PYL/RCAR proteins) was discovered independently by two groups [3,4]; the family comprises 14 members (PYR1 and PYL1-13) in *Arabidopsis thaliana* that share a characteristic START (star-related lipid transfer) domain [5]. Soon after this discovery, a large biochemical and structural research effort—focusing mainly on PYR1, PYL1, and PYL2—revealed the molecular mechanism behind the interactions between PYLs and downstream PP2Cs (type 2C protein phosphatases), and their inhibition of the phosphatase activity of PP2Cs such as ABI1, ABI2, and HAB1 [6–10]. Upon binding of ABA, two conserved loops in PYLs (termed as gate and latch [10] or CL2 and CL3 [6]) undergo significant conformational change, and thus create a protein surface suitable for PP2C association [6–10]. The substrate binding site for PP2C is blocked in the ABA–PYL–PP2C complex, which impairs the PP2C-mediated inhibition of downstream SnRK2 kinases, and leads to the accumulation of active SnRK2, possibly by autophosphorylation [6,9,10]. The activated SnRK2 can then activate the transcription and expression of relevant genes [11,12].

On the other hand, some members of this ABA receptor family may be able to constitutively interact with and inhibit PP2C [3,13]. Very recently, this was confirmed by Hao and colleagues through a systematic biochemical characterization of PYL proteins [14]. A subclass of PYL proteins, represented by PYL10 (UniProt accession: Q8H1R0), were able to constitutively bind and inhibit the phosphatase activity of PP2Cs, even in the absence of ABA. Their PP2Cs binding ability would be further stimulated by binding to ABA [14]. Their crystal structure of apo–PYL10 showed an open conformation in the CL2 loop, despite that a closed CL2 conformation was anticipated [14].

Here, we report the crystal structure of ligand-free PYL10 with a resolution of 3.0 Å. Interestingly, our apo–PYL10 structure showed a closed CL2 conformation, as expected by Hao and colleagues [14]. Further examination showed that the conformation of the CL2 loop was influenced by the CL3 loop of the other PYL10 molecule in the same asymmetric unit. To interpret the previously reported biochemical results, we proposed a putative two-conformation dynamical equilibrium model of PYL10. We also determined the crystal structure of the ABA–PYL10 complex with a resolution of 2.7 Å, which has not been reported previously.

2. Materials and methods

2.1. Protein expression, purification and crystallization

The PYL10 gene from *Arabidopsis thaliana* was cloned into the pET-21b(+) expression vector (Novagen) and expressed in

* Corresponding authors. Fax: +86 551 5591149 (F. Wu), +86 551 3600441 (C. Tian).
E-mail addresses: fmwu@hmfl.ac.cn (F. Wu), cltian@ustc.edu.cn (C. Tian).
[1] These authors contributed equally to this work.

0006-291X/$ - see front matter © 2012 Elsevier Inc. All rights reserved.
doi:10.1016/j.bbrc.2011.12.145

Table 1
Data collection and refinement statistics.

	Apo–PYL10	ABA–PYL10
Data collection		
Space group	P3121	P3121
Unit-cell parameters (Å, °):	$a = b = 80.47$, $c = 124.93$ $\alpha = \beta = 90$, $\gamma = 120$	$a = b = 68.33$, $c = 63.40$ $\alpha = \beta = 90$, $\gamma = 120$
Resolution (Å)	50.0–3.00 (3.05–3.00)	43.3–2.70 (2.76–2.70)
Number of unique reflections	9834	4929
Completeness (%)	98.2 (99.4)	99.2 (100)
Redundancy	4.2 (4.2)	5.3 (5.8)
Average $I/\sigma I$	12.7 (3.2)	40.6 (3.7)
R_{merge}[a] (%)	13.4 (52.1)	5.5 (29.6)
Refinement		
Resolution (Å)	46.5–3.00	59.17–2.70
R_{work} (No. of reflections)	22.0 (8679)	23.7 (4435)
R_{free} (No. of reflections)	28.8 (970)	27.4 (480)
R.M.S.D. bond lengths (Å)	0.010	0.010
R.M.S.D. bond angles (°)	1.403	1.402
Number of non-hydrogen atoms		
Protein	2451	1208
ABA	None	19
Water	34	11
Sulfate ion	5	None
Average B-factors (Å²)		
Protein	34.93	67.64
ABA	None	63.68
Water	27.88	65.93
Sulfate ion	46.91	None
Ramachandran plot[b]		
Favored (98%) regions	98.7%	97.4%
Allowed (>99.8%) regions	100%	100%

[a] $R_{merg} = |I_i - \langle I \rangle| / |I_i|$ where I_i is the intensity of the ith measurement, and $\langle I \rangle$ is the mean intensity for that reflection.
[b] Statistics for the Ramachandran plot from an analysis using MolProbity [21].

Escherichia coli strain BL21(DE3)RP (Stratagene). The transformed strain was incubated at 37 °C until the OD_{600} value reached 0.6–0.8; it was then induced using IPTG (isopropyl β-D-thiogalactopyranoside, Sigma) at 25 °C for 12 h. The harvested cells were lysed by sonication (300 cycles, 2 s per cycle, 1:2 pulse/pause at 30% amplitude of 750 W) in lysis buffer (70 mM Tris–HCl, pH 8.0, 300 mM NaCl) which was supplemented with 5.6 mM β-ME. The over-expressed proteins were purified using Ni-NTA affinity column (QIAGEN) and eluted by binding buffer (20 mM Tris–HCl, pH 8.0, 200 mM NaCl) supplemented with 300 mM imidazole and 5.6 mM β-ME. The protein was further purified by gel filtration chromatography (which was performed using a Superdex 75 10/300 GL column (GE healthcare), run on an ÄKTA system) in the buffer of 20 mM Tris–HCl, pH 8.0, 200 mM NaCl and 2 mM DTT. The fractionally collected proteins were concentrated using an Amicon Ultra filter (10,000 MWCO, Millipore).

The purified apo–PYL10 was concentrated to 7 mg/mL in 20 mM Tris–HCl, pH 8.0, 200 mM NaCl and 2 mM DTT. Crystals of apo- and ABA-bound PYL10 were grown at 295 K in 48-well plates (Xtal-Quest Co.), using the sitting-drop vapor diffusion method. One microliter of protein solution was mixed with an equal volume of reservoir solution, and the resulting droplet was equilibrated against 100 μL of reservoir solution. Apo–PYL10 crystallized in the well buffer containing 0.1 M Bis–Tris–HCl, pH 5.5, 0.2 M $(NH_4)_2SO_4$, and 25% PEG 3350. To obtain crystals of ABA-bound PYL10, apo–PYL10 was mixed with (+)-ABA (Sigma–Aldrich) at a molar ratio of 1:3, and concentrated to 9 mg/mL for co-crystallization. Crystals were obtained in the well buffer containing 0.1 M Bis–Tris–HCl, pH 6.5, and 20% PEG monoethyl ether 5000. The size and the shape of the crystals are presented in Supplementary Fig. S1.

2.2. Data collection, processing, structure determination and refinement

X-ray diffraction data were collected for both apo- and ABA-bound PYL10 at beamline BL17U at the SSRF (Shanghai Synchrotron Radiation Facility). Crystals were harvested, then soaked in a cryoprotectant solution containing crystallization buffer supplemented with 20% glycerol. The crystals were then flash-cooled in liquid nitrogen, and X-ray diffraction data was collected at 100 K. The observed reflections were reduced, merged and scaled with the program HKL-2000 [15].

Atomic coordinates of the apo-PYL2 (PDB ID: 3KDH) was used for molecular replacement with the program PHASER [16] into the data of apo–PYL10. The model completeness was done in COOT [17] and refinement was performed by REFMAC5 [18] with non-crystallographic symmetry (NCS) restraints in the early stage and CNS program (version 1.2) [19]. The structure of ABA-bound PYL10 was determined by molecular replacement with the program MOLREP [20] using the apo–PYL10 structure as the search model. The initial model was further refined using the program REFMAC5 [18], and rebuilt by using the σ_A-weighted electron-density maps with coefficients 2mFo−DFc and mFo−DFc in the program COOT [17]. The stereochemistry of the structure was checked by MolProbity [21]. The data collection and structure refinement statistics are summarized in Table 1.

3. Results

3.1. Overall structures of apo- and ABA-bound PYL10

Apo– and ABA–PYL10 were both crystallized in the P3121 space group. The structure of apo–PYL10 was refined to a resolution of 3.0 Å, with R_{work} and R_{free} values of 22.5% and 28.1%, respectively (Table 1). There were two molecules in each asymmetric unit (Supplementary Fig. S2). Similar to other members of the PYL family, the structure of PYL10 adopts a helix-grip fold (like the START domains [5]), which is mainly composed of seven anti-parallel β-strands and two α helices with the following topology: β1–α2–η1–β2–β3–β4–β5–β6–β7–α3 (η stands for a 3_{10}-helix) (Fig. 1A). The topology diagram was generated using PDBsum [22], and is shown in Supplementary Fig. S3. It should be mentioned that the N-terminal 24 residues—which correspond to the α1 helix in PYR1, PYL1 and PYL2—were missing in the density map. The structure of the ABA–PYL10 complex was determined by molecular replacement, using apo–PYL10 as the search model. The structure was refined to a resolution of 2.7 Å, with R_{work} and R_{free} values of 23.7% and 28.4%, respectively (see Table 1). It's noteworthy that there is large discrepancy of data quality between apo–PYL10 and ABA–PYL10. The Wilson B-factor of apo–PYL10 is only 37.6, while the Wilson B-factor of ABA–PYL10 is 78.0. So it is reasonable that average B-factor of apo–PYL10 is 29.8 and that of ABA–PYL10 is 66.4. One (+)-ABA molecule was coordinated in the putative PYL ligand-binding pocket (Fig. 1B) through hydrogen bond and *van der Waals* interactions, similar to the ligand binding mode of ABA to other known PYL family members. The carboxylate of ABA accepted one hydrogen bond from the side chain amine group of K56 (Fig. 1C). No water-mediated hydrogen bond was found, probably due to the relatively low resolution of the structure. The complex was also maintained via *van der Waals* contacts between ABA and the side-chains of F58, I59, L79, L83, I104, I106, L113, Y116, F155, V156, L159 and I160 (Fig. 1D). All of these residues were highly conserved in all 14 PYL proteins (Supplementary Fig. S4).

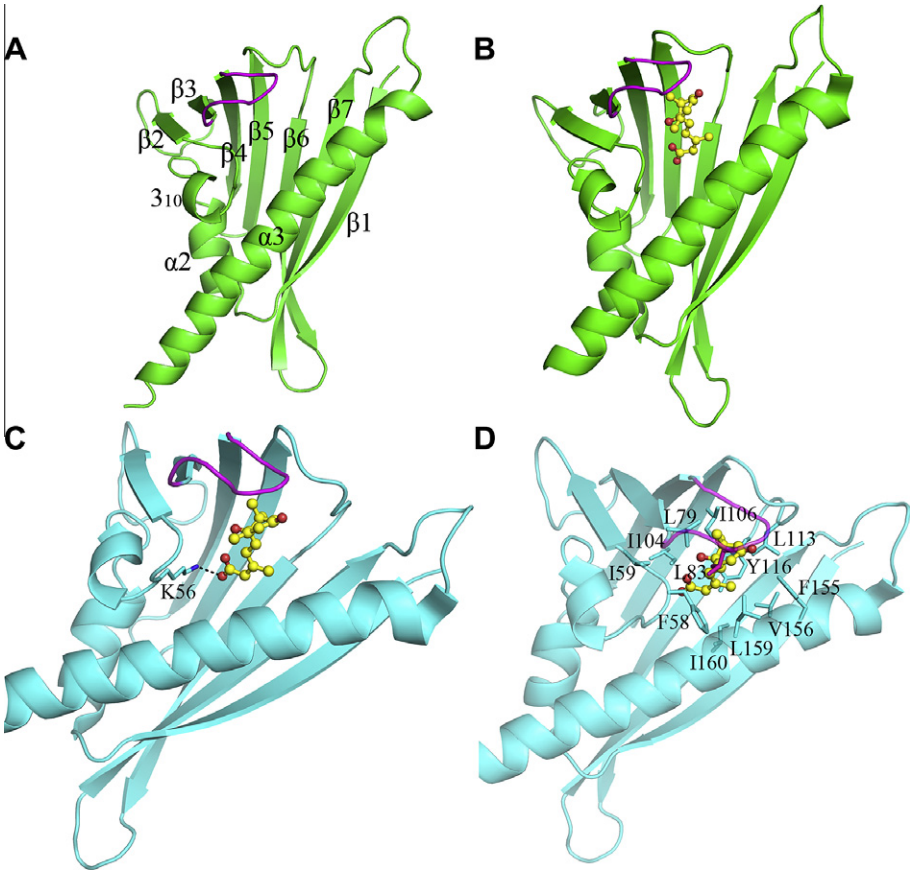

Fig. 1. Crystal structure of PYL10. Cartoon presentation of apo–PYL10 (A) and ABA–PYL10 (B). Detailed interactions between PYL10 and ABA via hydrogen bond (C) and *van der waals* interactions (D). The CL2 loops are shown in magenta, while the (+)-ABA molecule is represented in ball and stick model.

Very similar three-dimensional structures were observed when these two PYL10 structures (apo- and ABA-bound states) were superimposed (Fig. 2A) [even including the CL2 and CL3 loops [6] (or gate and latch loops [10])], with an RMSD value of 0.66 Å for 154 equivalent Cα atoms. Upon ABA binding, the backbone and side chains of the residues in the PYL10 gate loop moved only a short distance towards the ABA molecule (Fig. 2A). The PP2C binding surface of PYL10 showed only a slight change during the ABA binding process. In contrast, PYR1, PYL1, and PYL2 all underwent a pronounced conformational change from open state to closed state when one ABA molecule was bound, inducing a protein surface suitable for subsequent PP2C binding [6–10]. To further confirm the CL2 loop conformation in the apo–PYL10 structure at the resolution of 3.0 Å, the electron density omit map of the CL2 loop was presented in Supplementary Fig. S5.

3.2. Structural comparison between PYL members

A series of structural comparisons were made between PYL10 and other PYLs (Fig. 2B and C). The results showed that the apo form of PYL10 was quite different from the other three PYL members (PYR1/PYL1/PYL2) (Fig. 2B), while the ABA-bound form of PYL10 was very similar to the other three PYL members (PYR1/PYL1/PYL2) (Fig. 2C). The CL2 loops of both the apo and ABA-bound PYL10 were similar to the ABA-bound state of PYR1/PYL1/PYL2, since the CL2 loop was in a closed conformation in both apo- and ABA-bound PYL10. It has been reported that the closed conformation of the CL2 and CL3 loops provides a binding surface in PYL proteins for downstream PP2Cs [6,9,10]; our observations of similar CL2/CL3 conformations in both the apo- and ABA-bound states of PYL10 were in concert with several recent reports, which showed that some ABA receptors (PYL4-10, except the untested PYL7) could constitutively inhibit the phosphatase activity of one or several PP2Cs [3,13,14]. At first, we thought this might be the structural basis that explains the mechanism for the constitutive interaction between some PYLs (such as PYL5-10 and except PYL7) and PP2Cs.

While this manuscript was being prepared, Hao and colleagues [14] reported the crystal structures of apo–PYL10 and a PYL10–HAB1 complex. Interestingly, their apo–PYL10 structure was in an open conformation, while the authors initially expected a closed conformation which is presented in our apo-PYL10 structure. The two apo–PYL10 structures determined by Hao et al. (PDB ID: 3RT2) and by us (PDB ID: 3QTJ) are superimposed and shown in Fig. 2D. These two structures showed an RMSD value of 0.87 Å for 150 equivalent Cα atoms.

4. Discussion

Indeed, the apo–PYL10 structure in a closed conformation is more consistent with the biochemical results. Then, why an open conformation was obtained by Hao and colleagues? We noticed that these two research groups used different crystallization conditions to grow the crystals and the space groups of the obtained crystals were also different (Supplementary Table S1). Besides, there are two PYL10 molecules in each asymmetric unit in our structure, while only one is existed in the structure of Hao and colleagues. However, the two PYL10 molecules in the same

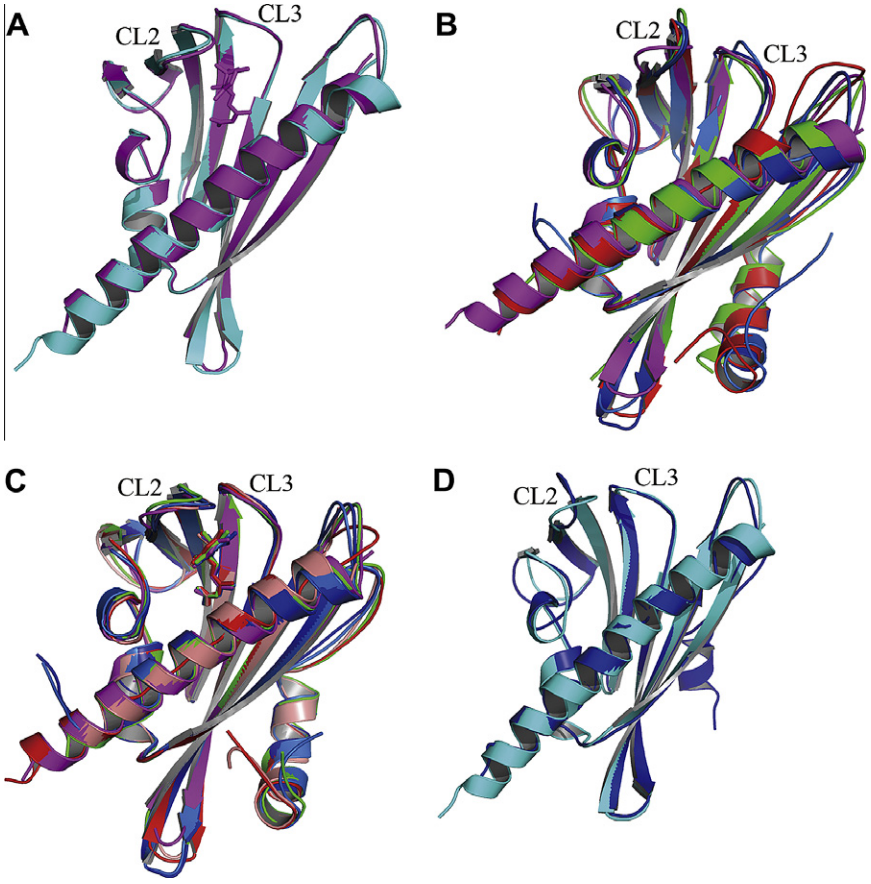

Fig. 2. Structural comparison between PYL members. (A) Structural superimposition of apo–PYL10 (Cyan) and ABA–PYL10 (Magenta). (B) Structural superimposition of apo-PYLs: PYR1 (Red, 3K3K:A, Nishimura et al. [8]), PYL1 (Green, 3KAY:A, Melcher et al. [10]), PYL2 (Blue, 3KAZ:A, Melcher et al. [10]; and Marine, 3KDH:A, Yin et al. [6]), and PYL10 (Magenta). (C) Structural superimposition of ABA-PYLs: PYR1 (Red, 3K3K:B, Nishimura et al. [8]; and Salmon, 3K90:A, Santiago et al. [7]), PYL1 (Green, 3JRS:A, Miyazono et al. [9]), PYL2 (Blue, 3KB0:A, Melcher et al. [10]; and Marine, 3KDI:A, Yin et al. [6]), and PYL10 (Magenta). (D) Structural superimposition of the apo–PYL10 structures obtained in this work (Cyan, 3QTJ) and by Hao et al. (Blue, 3RT2).

asymmetric unit or from two adjacent asymmetric units both formed a crystallographic dimer. Therefore, we carefully examined the dimer interface around the CL2 loop region of these two apo–PYL10 structures. In our apo–PYL10 structure, the CL2 loop of one PYL10 molecule interacts with the CL3 loop of the other PYL10 molecule. A hydrogen bond was formed between the side-chain amide of Arg112 and the backbone carbonyl oxygen of Leu83' (Fig. 3A). If the CL2 loop is in an open conformation, it will clash to the protruded long side-chain of Arg112 (Fig. 3A). In Hao's apo–PYL10 structure, the CL2 loop of one PYL10 molecule interacts with the CL4 loop of the other PYL10 molecule. A hydrogen bond was formed between the carbonyl oxygen of Gly82 and the side-chain amide of Asn147' (Fig. 3B). If the CL2 loop is in a closed conformation, it will clash to α3 helix (Fig. 3B). So the closed and open conformations of the CL2 loop in these two apo–PYL10 structures were both caused by crystal packing. It was shown that the bulky and hydrophobic residues (Leu79 and Leu83) guarding the ligand-binding pocket of PYL10 make hydrophobic contacts to CL1 and α3 to stabilize a closed CL2 conformation [14]. Given the fact that PYL10 exists as a monomer in solution [14], CL2 of the monomeric PYL10 is likely to be flexible in solution. Based on these results, it is reasonable to suggest that the apo–PYL10 structures obtained here and by Hao et al. represent two major conformations of a dynamical protein in solution. These two conformations probably both exist in solution. Here, we propose a hypothetical model (Fig. 4) that explains the constitutive interaction between PYL10 and PP2Cs and their binding affinity was extensively increased through the addition of ABA [14]. In solution, there should be a dynamical equilibrium between the open and closed conformations of PYL10. In the ligand-free state, the open conformation is the majority form, while the closed conformation is the minority form which contributes to its interaction with PP2Cs. The involvement of ABA, as well as the crystal packing force in our apo–PYL10 crystals, will disrupt the original equilibrium and induce a gradated shift in the equilibrium by conformational selection. Under this situation, the open conformation becomes the minority form, while the closed conformation becomes the majority form (Fig. 4). Probably, other conformations may also exist. In more detail, the above-mentioned closed conformation might also be divided into several sub-conformations, in order to interact with different PP2Cs or interact with the same PP2C with different binding affinities. The equilibrium shift between these sub-conformations when ABA and PP2C are both present might correspond to the increased PP2C binding ability and phosphatase activity inhibition. After all, more experiments need to be done to prove this hypothesis.

5. Accession numbers

The structure factors and coordinates have been deposited in the Protein Data Bank with accession codes 3UQH (apo–PYL10) and 3R6P (ABA–PYL10).

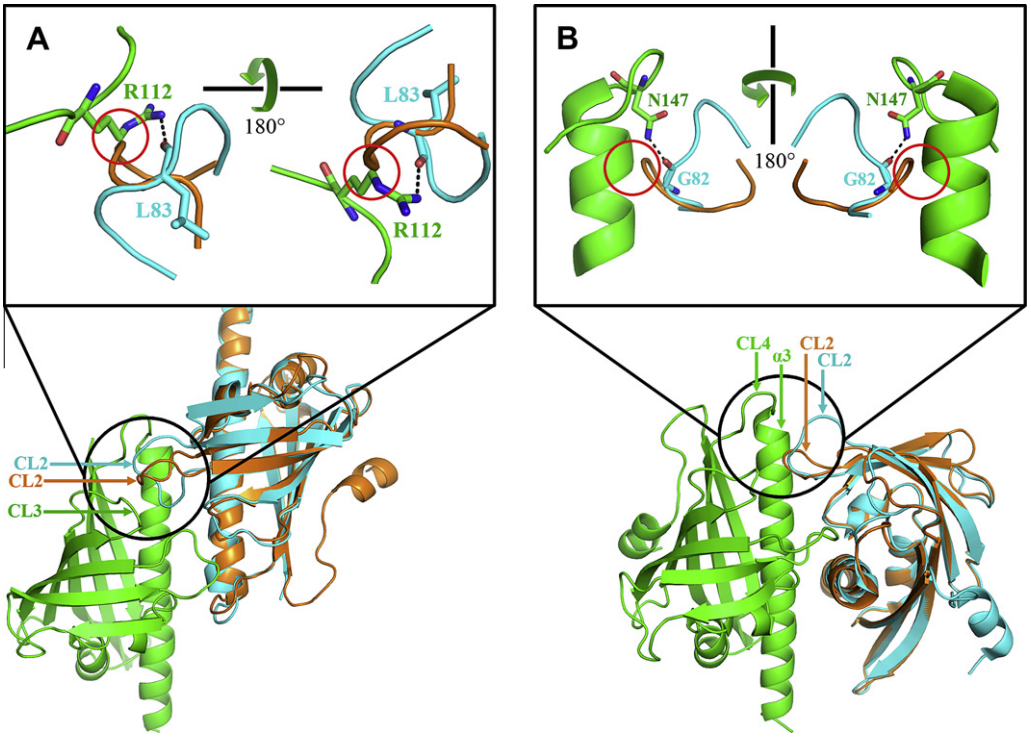

Fig. 3. The closed and open conformations of the CL2 loop in these two apo–PYL10 structures were both influenced by crystal packing. (A) The two closed-conformation PYL10 molecules in asymmetric unit are respectively shown in green and cyan. The open-conformation PYL10 structure solved by Hao and colleagues is shown in orange and superimposed onto the cyan PYL10 structure. (B) The two open-conformation PYL10 molecules from adjacent asymmetric units, which form a crystallographic dimer, are respectively shown in green and cyan. The closed-conformation PYL10 structure reported in this work is shown in orange and superimposed onto the cyan PYL10 structure. Crystal contacts around the CL2 loop are shown in details. Hydrogen bond is shown in black line of dashes. The red circles indicate the steric clash.

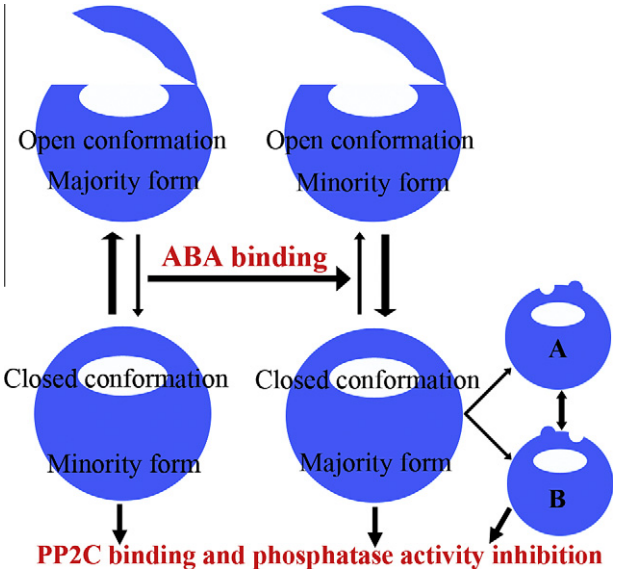

Fig. 4. The two-conformation dynamical equilibrium model of PYL10. There is an equilibrium between the open and closed conformations. ABA binding will substantially shift the equilibrium between these two conformations. In the ligand-free state, the closed conformation is the minority form which corresponds to its constitutive binding to PP2Cs. Once ABA is present, the closed conformation becomes the majority form. A and B stand for the sub-conformations of the closed state PYL10. More details are described in the main text.

Acknowledgments

We thank the staffs at SSRF (Shanghai Synchrotron Radiation Facility) beamline BL17U for their help during the data collection process. This work was supported by the Chinese Key Research Plan (No. 2011CB911104), a Chinese National High-Tech Research Grant (No. 2006AA02A321) to C.T. and the National Natural Science Foundation of China (No. 31100538) to F.W.

Appendix A. Supplementary data

Supplementary data associated with this article can be found, in the online version, at doi:10.1016/j.bbrc.2011.12.145.

References

[1] T. Hirayama, K. Shinozaki, Perception and transduction of abscisic acid signals: keys to the function of the versatile plant hormone ABA, Trends Plant Sci. 12 (2007) 343–351.
[2] A. Christmann, D. Moes, A. Himmelbach, Y. Yang, Y. Tang, E. Grill, Integration of abscisic acid signalling into plant responses, Plant Biol. 8 (2006) 314–325.
[3] S.Y. Park, P. Fung, N. Nishimura, D.R. Jensen, H. Fujii, Y. Zhao, S. Lumba, J. Santiago, A. Rodrigues, T.F. Chow, S.E. Alfred, D. Bonetta, R. Finkelstein, N.J. Provart, D. Desveaux, P.L. Rodriguez, P. McCourt, J.K. Zhu, J.I. Schroeder, B.F. Volkman, S.R. Cutler, Abscisic acid inhibits type 2C protein phosphatases via the PYR/PYL family of START proteins, Science 324 (2009) 1068–1071.
[4] Y. Ma, I. Szostkiewicz, A. Korte, D. Moes, Y. Yang, A. Christmann, E. Grill, Regulators of PP2C phosphatase activity function as abscisic acid sensors, Science 324 (2009) 1064–1068.
[5] L.M. Iyer, E.V. Koonin, L. Aravind, Adaptations of the helix-grip fold for ligand binding and catalysis in the START domain superfamily, Proteins 43 (2001) 134–144.
[6] P. Yin, H. Fan, Q. Hao, X.Q. Yuan, D. Wu, Y.X. Pang, C.Y. Yan, W.Q. Li, J.W. Wang, N. Yan, Structural insights into the mechanism of abscisic acid signaling by PYL proteins, Nat. Struct. Mol. Biol. 16 (2009) 1230–1236.
[7] J. Santiago, F. Dupeux, A. Round, R. Antoni, S.Y. Park, M. Jamin, S.R. Cutler, P.L. Rodriguez, J.A. Marquez, The abscisic acid receptor PYR1 in complex with abscisic acid, Nature 462 (2009) 665–668.
[8] N. Nishimura, K. Hitomi, A.S. Arvai, R.P. Rambo, C. Hitomi, S.R. Cutler, J.I. Schroeder, E.D. Getzoff, Structural mechanism of abscisic acid binding and signaling by dimeric PYR1, Science 326 (2009) 1373–1379.
[9] K. Miyazono, T. Miyakawa, Y. Sawano, K. Kubota, H.J. Kang, A. Asano, Y. Miyauchi, M. Takahashi, Y. Zhi, Y. Fujita, T. Yoshida, K.S. Kodaira, K. Yamaguchi-Shinozaki,

M. Tanokura, Structural basis of abscisic acid signalling, Nature 462 (2009) 609–614.
[10] K. Melcher, L.M. Ng, X.E. Zhou, F.F. Soon, Y. Xu, K.M. Suino-Powell, S.Y. Park, J.J. Weiner, H. Fujii, V. Chinnusamy, A. Kovach, J. Li, Y.H. Wang, J.Y. Li, F.C. Peterson, D.R. Jensen, E.L. Yong, B.F. Volkman, S.R. Cutler, J.K. Zhu, H.E. Xu, A gate-latch-lock mechanism for hormone signalling by abscisic acid receptors, Nature 462 (2009) 602–608.
[11] J.J. Weiner, F.C. Peterson, B.F. Volkman, S.R. Cutler, Structural and functional insights into core ABA signaling, Curr. Opin. Plant Biol. 13 (2010) 495–502.
[12] Y. Fujita, K. Nakashima, T. Yoshida, T. Katagiri, S. Kidokoro, N. Kanamori, T. Umezawa, M. Fujita, K. Maruyama, K. Ishiyama, M. Kobayashi, S. Nakasone, K. Yamada, T. Ito, K. Shinozaki, K. Yamaguchi-Shinozaki, Three SnRK2 protein kinases are the main positive regulators of abscisic acid signaling in response to water stress in Arabidopsis, Plant Cell Physiol. 50 (2009) 2123–2132.
[13] N. Nishimura, A. Sarkeshik, K. Nito, S.Y. Park, A. Wang, P.C. Carvalho, S. Lee, D.F. Caddell, S.R. Cutler, J. Chory, J.R. Yates, J.I. Schroeder, PYR/PYL/RCAR family members are major in-vivo ABI1 protein phosphatase 2C-interacting proteins in Arabidopsis, Plant J. 61 (2010) 290–299.
[14] Q. Hao, P. Yin, W. Li, L. Wang, C. Yan, Z. Lin, J.Z. Wu, J. Wang, S.F. Yan, N. Yan, The molecular basis of ABA-independent inhibition of PP2Cs by a subclass of PYL proteins, Mol. Cell 42 (2011) 662–672.
[15] Z. Otwinowski, W. Minor, Processing of X-ray diffraction data collected in oscillation mode, Method Enzymol. 276 (1997) 307–326.
[16] A.J. McCoy, R.W. Grosse-Kunstleve, P.D. Adams, M.D. Winn, L.C. Storoni, R.J. Read, Phaser crystallographic software, J. Appl. Crystallogr. 40 (2007) 658–674.
[17] P. Emsley, K. Cowtan, Coot: model-building tools for molecular graphics, Acta Crystallogr. D Biol. Crystallogr. 60 (2004) 2126–2132.
[18] G.N. Murshudov, A.A. Vagin, E.J. Dodson, Refinement of macromolecular structures by the maximum-likelihood method, Acta Crystallogr. D Biol. Crystallogr. 53 (1997) 240–255.
[19] A.T. Brunger, P.D. Adams, G.M. Clore, W.L. DeLano, P. Gros, R.W. Grosse-Kunstleve, J.S. Jiang, J. Kuszewski, M. Nilges, N.S. Pannu, R.J. Read, L.M. Rice, T. Simonson, G.L. Warren, Crystallography and NMR system: a new software suite for macromolecular structure determination, Acta Crystallogr. D Biol. Crystallogr. 54 (1998) 905–921.
[20] A. Vagin, A. Teplyakov, MOLREP: an automated program for molecular replacement, J. Appl. Crystallogr. 30 (1997) 1022–1025.
[21] V.B. Chen, W.B. Arendall 3rd, J.J. Headd, D.A. Keedy, R.M. Immormino, G.J. Kapral, L.W. Murray, J.S. Richardson, D.C. Richardson, MolProbity: all-atom structure validation for macromolecular crystallography, Acta Crystallogr. D Biol. Crystallogr. 66 (2010) 12–21.
[22] R.A. Laskowski, Enhancing the functional annotation of PDB structures in PDB sum using key figures extracted from the literature, Bioinformatics 23 (2007) 1824–1827.